

# Dynamic and static measurements on epitaxial Fe/Si/Fe

Bijoy K. Kuanr<sup>a)</sup>

*Department of Physics, University of Colorado at Colorado Springs, Colorado Springs, Colorado 80918*

M. Buchmeier, D. E. Buergler, and P. Gruenberg

*Forschungszentrum Juelich GmbH, Juelich, Germany*

R. Camley and Z. Celinski

*Department of Physics, University of Colorado at Colorado Springs, Colorado Springs, Colorado 80918*

(Received 7 October 2002; accepted 13 January 2003; published 30 June 2003)

Strong antiferromagnetic interlayer exchange coupling across an insulating spacer is in increasing demand for high-density magnetic recording. We report here on the interlayer exchange coupling of epitaxial Fe(8 nm)/Si(*t*)/Fe(10 nm) trilayers as a function of Si thickness studied by ferromagnetic resonance (FMR), Brillouin light scattering, and magneto optic Kerr effect (MOKE) measurement techniques. A very strong antiferromagnetic (AFM) interlayer exchange coupling ( $>6$  erg/cm<sup>2</sup>) was observed at a spacer Si thickness of 0.7 nm. The bilinear  $J_1$  and biquadratic  $J_2$  coupling constants were determined from (i) the fitting of the angular variation of the resonance field ( $H_{\text{res}}$ ) in FMR experiments, (ii) the field variation of the frequencies of the Damon–Eshbach surface modes (both optic and acoustic) in BLS measurements, and (iii) the fitting of longitudinal MOKE hysteresis loops. We obtain a higher  $H_{\text{res}}$  along the easy axis than along the hard axis and the magnetizations of the two Fe films are canted. The eightfold-like symmetry of  $H_{\text{res}}$  as a function of the angle observed at room temperature is due to the competition between the Fe fourfold anisotropy and AFM interfacial coupling energy. This behavior vanishes at low temperatures due to a strong increase of AFM coupling (especially  $J_2$ ) in comparison to fourfold in-plane anisotropy. From the fitting of the temperature dependent FMR data, we obtain the temperature variation of the bilinear and biquadratic exchange coupling constants. We distinguish the existence of canted magnetization states at resonance by fitting the experimental  $H_{\text{res}}$  versus  $\theta_H$  data to the model calculation. © 2003 American Vacuum Society. [DOI: 10.1116/1.1562181]

## I. INTRODUCTION

Studies of magnetic interactions between two ferromagnetic films separated by a nonmagnetic spacer have been a subject of extensive research for the past two decades. Elements like Cr, Cu, Ag, and Pd were extensively studied as spacers<sup>1,2</sup> to understand the nature and strength of interlayer exchange coupling. Typically the observed coupling strength was smaller than 1 erg/cm<sup>2</sup>. For practical applications such as high density recording, a strong antiferromagnetic (AFM) exchange coupling across insulating spacer material is desirable. The Fe/Si exchange coupled multilayer system is a strong potential candidate due to its unusually high antiferromagnetic exchange coupling.<sup>3–8</sup> This coupling exhibits a strong exponential decay versus spacer thickness.<sup>5,6</sup> It was suggested before that in the Fe/Si/Fe system most of the Si had turned into metallic FeSi<sup>5</sup> due to Fe diffusion.

Ferromagnetic and antiferromagnetic exchange coupling in magnetic multilayers are frequently studied by two dynamical techniques—ferromagnetic resonance (FMR) and Brillouin light scattering (BLS).<sup>1,2,9</sup> The modes observed by FMR and BLS<sup>9–11</sup> (acoustic and optic branches) are sensitive to the magnetic energy within each ferromagnetic film as well as the interlayer exchange coupling across the nonmagnetic spacer. In addition, the magneto optic Kerr effect (MOKE) technique, which measures the static properties of

the material, is widely used to determine the strength of antiferromagnetic coupling between layers. To determine ferromagnetic coupling strengths by MOKE one has to turn to a spin engineering technique similar to one developed by Parkin.<sup>12</sup>

We have studied the bilinear ( $J_1$ ) and biquadratic ( $J_2$ ) exchange coupling of Fe/Si/Fe trilayers as a function of Si thickness and temperature. We use dynamic (FMR and BLS) and static (MOKE) techniques and the results obtained by the different techniques show good agreement. We find extremely strong antiferromagnetic coupling at a Si thickness of 0.7 nm for room temperature. The magnitude of the biquadratic coupling constant decreases very rapidly as the temperature increases.

## II. EXPERIMENTS

Epitaxial Fe/Si/Fe trilayers, with Si thickness between 0.6 and 1.2 nm, were grown by molecular beam epitaxy (MBE) on a GaAs(100)/Fe(1 nm)/Ag(150 nm) substrate-buffer system. The background pressure was better than  $10^{-9}$  mbar. The deposition rate was maintained at 0.1 Å/s for both Fe and Si. During the depositions of Fe and Si, the substrate was kept at room temperature. The thickness and deposition rate were controlled by a calibrated quartz-crystal monitor. The samples were characterized *in situ* by Auger electron spectroscopy (AES), low energy electron diffraction (LEED), and reflection high-energy electron diffraction (RHEED). Both

<sup>a)</sup>Electronic mail: bkuanr@brain.uccs.edu

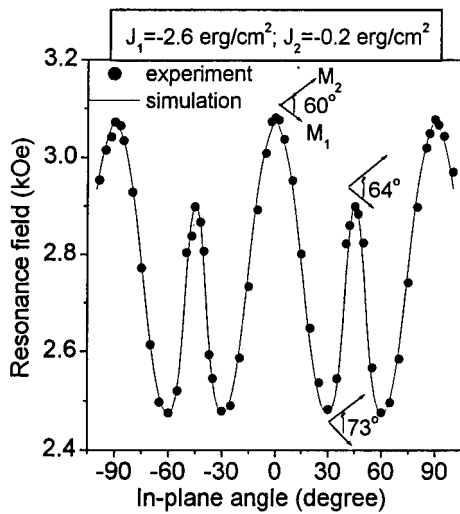


FIG. 1. In-plane angular ( $\theta_H$ ) variation of acoustic resonance field ( $H_{\text{res}}$ ) at room temperature (experimental: ● and theoretical: —) for antiferromagnetically coupled Fe(8 nm)/Si(1.0 nm)/Fe(10 nm) trilayer film studied by FMR at 24 GHz. The insets show the Fe magnetization directions at different resonance field values.

RHEED and LEED indicated epitaxial growth of Fe and Si layers. The samples were covered with a 50 nm ZnS antireflection layer that also prevents oxidation of the top Fe layer.

The magnetic properties of the exchange coupled samples were characterized through the study of resonance field modes (acoustic and optic) as a function of in-plane field angle with 24 and 35 GHz FMR spectrometers. A closed cycle helium Dewar was used to cool the sample from room temperature down to 25 K. The BLS experiments were performed at room temperature, in the backscattering geometry, with a (2×3) pass tandem Fabry–Perot interferometer.<sup>1,9</sup> The inelastically scattered light, corresponding to both the Stoke and the anti-Stoke, was recorded using an avalanche diode and a multichannel analyzer PC card. The free spectral range of the interferometer was  $\pm 50$  GHz. The wavelength  $\lambda = 532$  nm of the incident laser light together with an angle of incidence of  $45^\circ$  resulted in an in-plane magnon wave vector  $k_{\parallel} = 1.65(10^7) \text{ m}^{-1}$ . A variable external field with a maximum strength of 7 kOe was applied in the sample plane and normal to the magnon wave vector. The surface modes of acoustic and optic spin waves were recorded on both the Stokes and the anti-Stokes sides of the spectrum. In addition, we used longitudinal MOKE measurements to record the hysteresis curves of the samples at room temperature.

### III. RESULTS AND DISCUSSION

Figure 1 shows the in-plane angular variation of the resonance fields for the acoustic modes,  $H_{\text{res}}(\theta_H)$  for a Fe(8 nm)/Si(1 nm)/Fe(10 nm) sample, measured at 24 GHz and at room temperature. The dots are experimental data and the solid lines are the results of theoretical calculations for the resonance field positions.<sup>9–11</sup> The eightfold-like symmetry for  $H_{\text{res}}(\theta_H)$  (four peaks from  $-90^\circ$  to  $+90^\circ$ ) is clearly apparent at room temperature. Surprisingly, we observed a

higher  $H_{\text{res}}$  along the direction which is normally the Fe easy axis ( $0, \pm 90^\circ$ ) than along the direction which is normally the hard axis ( $\pm 45^\circ$ ).

To interpret these data we used a rather complex dispersion relation calculated for a strongly AFM coupled trilayer with the field applied in the sample plane.<sup>13</sup> The equilibrium position of the magnetization vector was obtained for each applied field from the total free energy<sup>9,11,13</sup> (Zeeman, demagnetizing, cubic anisotropy, and exchange coupling energy) expression. Our energy minimization process<sup>9,10</sup> can be used for any AFM exchange coupling strength and for any magnetic state<sup>13</sup> (saturated or unsaturated) of the sample to obtain the resonance field positions. The solid line in Fig. 1 shows the results of this calculation. The coupling constants obtained from the best fit to the experimental data are  $J_1 = -2.6 \text{ erg/cm}^2$  and  $J_2 = -0.2 \text{ erg/cm}^2$ . The values of the cubic anisotropy and magnetization obtained from the fit are close to room temperature bulk values.

The acoustic resonance seen in Fig. 1 occurs at an unsaturated state, i.e., the magnetizations in the individual films do not point in the direction of the external static field, but are canted. The canting angle (angle between  $\mathbf{M}_1$  and  $\mathbf{M}_2$ ) obtained from the simulation is  $60^\circ$  when the applied field is along the easy axis ( $\theta_H = 0^\circ$ ), increases to  $73^\circ$  when  $\theta_H = 28^\circ$  (near the minimum for  $H_{\text{res}}$ ), and then decreases to  $64^\circ$  for the applied field along the (usual) hard axis ( $\theta_H = 45^\circ$ ). The insets in Fig. 1 show the direction of Fe magnetization vectors  $\mathbf{M}_1$  and  $\mathbf{M}_2$ .

The observed eightfold-like symmetry is due to the strong competition between the fourfold anisotropy energy of Fe and the strong antiferromagnetic coupling energy due to the Si spacer. It is easy to immediately conclude that the AFM coupling energy is stronger than the cubic energy because  $H_{\text{res}}(0^\circ) > H_{\text{res}}(45^\circ)$ .

Normally it is necessary to have measurements on both the acoustic and optic modes in order to obtain  $J_1$  and  $J_2$ . Due to magnetic field limitations we were not able to measure the optic resonance. Nonetheless, the excellent agreement of the experimental  $H_{\text{res}}(\theta_H)$  data with the model calculation<sup>10,11,13</sup> demonstrates that it is possible to obtain the coupling constants  $J_1$  and  $J_2$  from the angular variation of acoustic resonance without the optic resonance because the Fe magnetizations in the trilayer are in a canted state.

Figure 2 shows  $H_{\text{res}}(\theta_H)$  data for the same sample measured at room temperature with the 35 GHz FMR system. For the fields used in this experiment (4.8 to 6 kOe) both  $\mathbf{M}_1$  and  $\mathbf{M}_2$  are aligned along the applied magnetic field (shown in the inset to this figure) and one measures the normal acoustic resonance. Therefore the eightfold-like symmetry observed at 24 GHz vanishes at this frequency. Figure 2 shows a standard fourfold symmetry expected for (100) Fe, with the easy-magnetization axis along  $0^\circ$  and hard along  $45^\circ$ , and with zero uniaxial anisotropy. The solid line to the figure was obtained from the model calculation<sup>10,11,13</sup> using a  $g$  factor of 2.08, which yields the following magnetic parameters;  $H_K = 0.55$  kOe and  $4\pi M_S = 21$  kOe, in agreement with 24 GHz FMR results. Also, at this frequency we were not

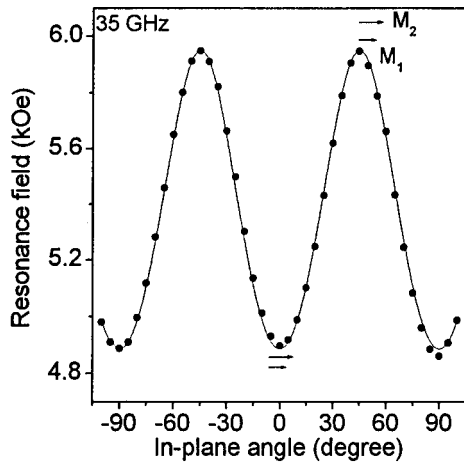


FIG. 2. FMR  $H_{\text{res}}(\theta_H)$  data obtained from a 35 GHz FMR system [experimental (●) and theoretical (—)] for the Fe(8 nm)/Si(1.0 nm)/Fe(10 nm) trilayer.

able to measure the optic resonance due to the unavailability of a strong magnetic field.

Figure 3 shows the deduced coupling coefficients  $J_1$  and  $J_2$  as a function of Si spacer thickness ( $t$ ) for Fe(8 nm)/Si( $t$ )/Fe(10 nm) trilayers. The coefficients were obtained from room temperature FMR measurements at 24 GHz. We observed antiferromagnetic (AFM) exchange coupling for all studied thicknesses of Si spacers. The exchange coupling constants were derived from our  $H_{\text{res}}(\theta_H)$  data. At a spacer thickness of 0.6 nm, the coupling is dominantly biquadratic; with  $J_1 = -3.4$  erg/cm<sup>2</sup> and  $J_2 = -2.65$  erg/cm<sup>2</sup>, which is among the strongest biquadratic coupling ever found. The AFM coupling strength attained a maximum at 0.7 nm spacer thickness with  $J_1 = -6.5$  erg/cm<sup>2</sup> and  $J_2 = -1.1$  erg/cm<sup>2</sup>. Both  $J_1$  and  $J_2$  decrease rapidly in magnitude for larger Si thicknesses (1.0 and 1.2 nm). It was observed that  $J_2$  remains consistently smaller (in magnitude) than  $J_1$  and decays faster. The strong decrease of bilinear coupling at smaller Si thickness could be explained in terms

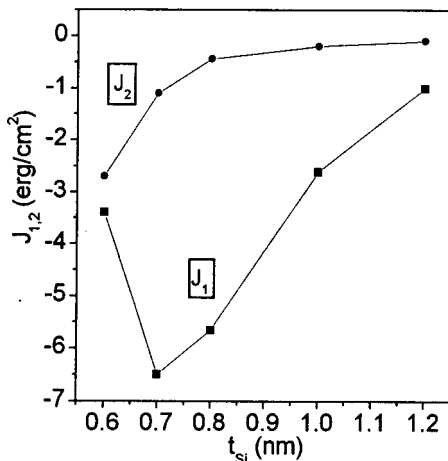


FIG. 3. Room temperature coupling strength of bilinear ( $J_1$ ) and biquadratic ( $J_2$ ) constants as a function of Si spacer thickness.

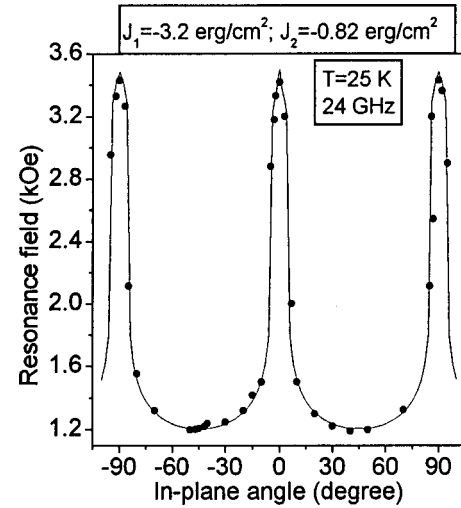


FIG. 4. Acoustic resonance field ( $H_{\text{res}}$ ) vs in-plane angle ( $\theta_H$ ) (experimental; ● and theoretical; —) for Fe(8 nm)/Si(1.0 nm)/Fe(10 nm) trilayer at 25 K.

of Slonczewski's<sup>14</sup> theory by a competition of ferromagnetic (FM) (possibly due to pinholes) coupling and antiferromagnetic (AFM) interlayer coupling. The fast decay of  $J_2$  with increasing spacer thickness is in agreement with this mechanism,<sup>14</sup> for example, because the number of pinholes decreases with increasing thickness of the Si spacer. The observed weak biquadratic coupling for Si thickness above 0.8 nm is in agreement with smooth decay of  $J_1$ , as predicted by Slonczewski.<sup>14</sup>

Figure 4 shows the  $H_{\text{res}}(\theta_H)$  data for the same trilayer sample at 25 K. The figure depicts a fourfold symmetry, but with a higher  $H_{\text{res}}$  along the easy axis ( $0^\circ$ ) compared to that along the hard axis ( $45^\circ$ ). The coupling constants derived from the resonance fit<sup>10,11,13</sup> are  $J_1 = -3.2$  erg/cm<sup>2</sup> and  $J_2 = -0.82$  erg/cm<sup>2</sup> along with a small increase of the effective anisotropy field value (0.67 kOe). At 25 K, the resonance was observed at a canted state. However, the AFM coupling energy completely dominates the cubic anisotropy energy and therefore the eightfold-like symmetry, observed at room temperature, vanished at this low temperature.

Figure 5 compiles both  $J_1$  and  $J_2$  coupling constants for the Fe(8 nm)/Si(1.0 nm)/Fe(10 nm) trilayer sample from 25 to 300 K obtained from 24 GHz FMR measurements. We observed that both  $J_1$  and  $J_2$  decrease with increasing temperature ( $T$ ). However, the temperature dependence of  $J_2$  is much stronger than that of  $J_1$ . The biquadratic coupling increases fourfold from room temperature down to 25 K, whereas the bilinear coupling increases only slightly by a factor of 1.25 at 25 K to its value at room temperature.

The slow decrease of  $J_1$  with temperature could be associated with reduced magnetization of Fe. For example, the magnetization and the linear exchange coupling constant,  $J_1$ , both saturate below 100 K. The temperature dependence of  $J_1$  for insulating and metallic spacers can be described by the quantum interference model of Bruno.<sup>16</sup> We discuss our results in the light of available theories.<sup>14-16</sup> According to Slonczewski,<sup>15</sup> the increase of  $J_1$  and  $J_2$  can be mediated by

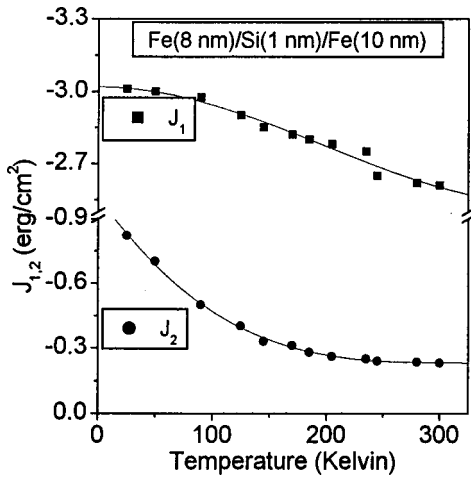


Fig. 5. Temperature dependence (25–300 K) of bilinear ( $J_1$ ) and biquadratic ( $J_2$ ) coupling strengths for Fe(8 nm)/Si(1.0 nm)/Fe(102 nm) trilayer film. The solid lines serve as a guide to the eye only.

loose spins present inside the spacer or adjacent to the Fe/Si interface, which can couple to both Fe layers via indirect exchange. Another possibility<sup>14</sup> resulting in a strong decrease of  $J_2$  with temperature can be due to thickness fluctuations of the Si spacer. This causes a competition between FM and AFM coupling for neighboring regions, which may lead to a frustration of coupling. Strijkers *et al.*<sup>6</sup> favored the loose spin model<sup>15</sup> to interpret their data of strong exponential decay of  $J_2$ . On the contrary, Fullerton *et al.*<sup>3</sup> discussed their strong temperature dependence of biquadratic coupling data by spatial or compositional fluctuations at interfaces termed as a fluctuation mechanism by Slonczewski.<sup>14</sup> For all known biquadratic coupling mechanism, loose spin models,<sup>15</sup> the fluctuation model<sup>14</sup> and the intrinsic higher order term<sup>16</sup>  $-J_2$  increases monotonically upon cooling.

In Fig. 6 we show the magnetic field dependence of BLS

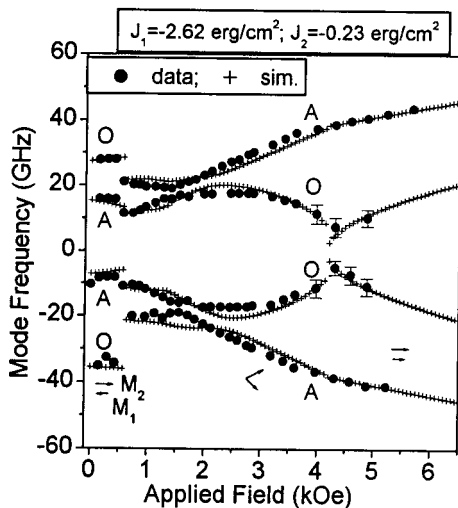


Fig. 6. BLS mode frequencies vs magnetic field for the Fe(8 nm)/Si(1.0 nm)/Fe(10 nm) trilayer showing the acoustic (marked A) and optic (marked O) branches on both Stokes and anti-Stokes sides. The plus signs (+) are the theoretical calculation.

mode frequencies for the Fe(8 nm)/Si(1 nm)/Fe(1 nm) trilayer film with the magnetic field applied along the easy axis of the film. The two modes shown here (closed circles) are the acoustic and optic surface modes.<sup>1,9,11</sup> In a typical BLS spectrum the acoustic mode is identified as the higher intensity mode and the optic mode as the lower intensity mode. The acoustic modes are marked as “A” and the optic modes as “O” in the figure. The evolution of the spectra with magnetic field corresponds to changes in magnetization directions of  $\mathbf{M}_1$  and  $\mathbf{M}_2$ . As the applied field is increased from zero, the two magnetizations change from an antiparallel configuration to a spin flop or canted state, and finally at high field to parallel alignment.

For the antiparallel alignment, the frequency of the optic mode is higher than that of the acoustic mode. A strong asymmetry of the Stoke and the anti-Stoke spectra reflects strong AFM coupling with antiparallel alignment of Fe magnetizations. The asymmetry and the sudden jump of mode frequencies reflect the transition of magnetization alignment from antiparallel to spin flop at 0.6 kOe and then from spin flop to parallel at 4.2 kOe magnetic field. In the spin flop region, the rotation of magnetizations towards field direction is accompanied by a crossing of the spin wave modes. From the theoretical simulations it is identified that the crossing point of the spin wave modes corresponds to an exact 90° alignment between  $\mathbf{M}_1$  and  $\mathbf{M}_2$ .

At large applied fields  $\mathbf{M}_1$  and  $\mathbf{M}_2$  become parallel. In this case the difference in frequency between the acoustic and optic modes is a measure of the exchange coupling energy between the two ferromagnetic layers. We fitted the experimental results to the model calculation<sup>9–11</sup> to obtain the exchange coupling strengths  $J_1$  and  $J_2$ . The quantitative evaluation of coupling constants is done by considering the equation of motion and boundary conditions.<sup>9–11</sup> The plus sign (+) indicating the results of the theoretical calculations were generated from a Levenberg–Marquardt fit to the experimental data. The strength of  $J_1$  and  $J_2$  obtained from the BLS data are  $-2.62$  and  $-0.23$  erg/cm<sup>2</sup>, respectively. The BLS results and the FMR results are in good agreement for all the other samples with different Si thicknesses.

The BLS and FMR measurements above probe the dynamical properties of the samples. It is important to know if the static properties can be explained using the same parameters that apply to the dynamical system. We used MOKE to study the static magnetization as a function of applied field. The experimental easy and hard axis MOKE hysteresis loops are fitted<sup>11</sup> by considering the anisotropy ( $K_1$ ), bilinear ( $J_1$ ), biquadratic ( $J_2$ ), and Zeeman energies. The hysteresis loops are simulated by minimizing the total free energy of the system with respect to the magnetization directions of the two Fe layers for each value of  $H$ . We can obtain both  $J_1$  and  $J_2$  coupling constants due to the existence of two plateaus in the hysteresis loops and the determined values are within 5% of the FMR and BLS results.

#### IV. CONCLUSION

We investigated Fe/Si/Fe trilayers with strong antiferromagnetic exchange coupling by FMR and BLS. Both tech-

niques provide the possibility to determine the bilinear ( $J_1$ ) and biquadratic ( $J_2$ ) coupling constants. The  $H_{\text{res}}(\theta_H)$  curves were well understood from a theoretical calculation suited for strong AFM coupling. The observed eightfold-like symmetry is due to competition between strong AFM coupling energy and cubic anisotropy energy and results in an unusual situation where  $H_{\text{res}}$  is higher along the (normally) easy-axis direction compared to that along the hard axis. This behavior vanished at low temperature where AFM coupling energy completely dominates the anisotropy energy. At room temperature we obtain  $J_1 = -2.6 \text{ erg/cm}^2$  and  $J_2 = -0.2 \text{ erg/cm}^2$ . These results are in excellent agreement with those obtained from fitting the mode frequencies in BLS experiments. We also find the behavior of  $J_1$  and  $J_2$  as a function of temperature and show that the magnitude of  $J_2$  decreases rapidly as the temperature increases.

## ACKNOWLEDGMENTS

The work at UCCS was supported by the US ARO (DAAG19-00-1-0146 and DAAD-19-02-1-0174) and by HGF-Strategiefonds at FZ-Juelich.

- <sup>1</sup>P. Gruenberg, R. Schreiber, Y. Pang, M. B. Brodsky, and H. Sower, *Phys. Rev. Lett.* **57**, 2442 (1986).
- <sup>2</sup>B. Heinrich and J. A. C. Bland, *Ultrathin Magnetic Structures, I, II* (Springer, Berlin, 1994).
- <sup>3</sup>E. E. Fullerton, J. E. Mattson, S. R. Lee, C. H. Sowers, Y. Y. Huang, G. Felcher, S. D. Bader, and F. T. Parker, *J. Magn. Magn. Mater.* **117**, L301 (1992); *Phys. Rev. B* **53**, 5112 (1996).
- <sup>4</sup>A. Chaiken, R. P. Michel, and M. A. Wall, *Phys. Rev. B* **53**, 5518 (1996).
- <sup>5</sup>J. J. de Vries, J. Kohlhepp, F. J. A. den Broeder, R. Coehoorn, R. Jungblut, A. Reinders, and W. J. M. de Jonge, *Phys. Rev. Lett.* **78**, 3023 (1997).
- <sup>6</sup>G. J. Strijkers, J. T. Kohlhepp, H. J. M. Swagten, and W. J. M. de Jonge, *J. Appl. Phys.* **87**, 5452 (2000); *Phys. Rev. Lett.* **84**, 1812 (2000).
- <sup>7</sup>R. R. Gareev, D. E. Bürgler, M. Buchmeier, D. Olligs, R. Schreiber, and P. Grünberg, *Phys. Rev. Lett.* **87**, 157202 (2001).
- <sup>8</sup>P. Gruenberg, D. E. Bürgler, D. Olligs, R. R. Gareev, M. Buchmeier, B. K. Kuanr, and R. Schreiber, *J. Phys. D* **35**, 2403 (2002).
- <sup>9</sup>B. K. Kuanr, M. Buchmeier, D. E. Bürgler, and P. Gruenberg, *J. Appl. Phys.* **91**, 7209 (2002).
- <sup>10</sup>M. Buchmeier, B. K. Kuanr, R. R. Gareev, D. E. Bürgler, and P. Gruenberg (unpublished).
- <sup>11</sup>S. M. Rezende, C. Chesman, M. A. Lucena, A. Azevedo, F. M. de Aguiar, and S. S. P. Parkin, *J. Appl. Phys.* **84**, 958 (1998).
- <sup>12</sup>S. S. P. Parkin and D. Mauri, *Phys. Rev. B* **44**, 7131 (1991).
- <sup>13</sup>J. Geshev, L. G. Pereira, and J. E. Schmidt, *Physica B* **320**, 169 (2002).
- <sup>14</sup>J. C. Slonczewski, *Phys. Rev. Lett.* **67**, 3172 (1991).
- <sup>15</sup>J. C. Slonczewski, *J. Appl. Phys.* **73**, 5957 (1993).
- <sup>16</sup>P. Bruno, *Phys. Rev. B* **52**, 411 (1995).